This the unedited accepted format of this article. Please site this article as: Kamyabi M, Kamyabi A, On the Dynamic Contact Angle in Capillary Flows. Journal of Chemical and Petroleum Engineering.
DOI: 10.22059/jchpe.2021.318146.1346

On the Dynamic Contact Angle in Capillary Flows

Mohammadmahdi Kamyabi[1a], Ata Kamyabi[b]

[a,1] *Department of Chemical Engineering ,College of Engineering, Vali-e-Asr University of Rafsanjan, Rafsanjan, Iran*

[b]*Department of Chemical Engineering, College of Engineering, Shahid Bahonar University of Kerman, Kerman, Iran*

ABSTRACT

The displacement of the contact line (CL) between two arbitrary immiscible flowing fluids was modeled. The present model is valid for a wide range of viscosity ratios of the phases. This is while the previously developed models reported in the literature were devoted to special cases *i.e.* high viscosity fluid pushing the low viscosity fluid. The present model reveals a direct relationship among the dynamic contact angle, the dimensionless pressure difference in the channel/tube, the Capillary numbers of both phases, and the characteristic length ratios of the channel/tube. The model was validated through the agreement of its predictions for the dynamic contact angle with the available data for a case of water-air flow inside a tube. Then, it was applied to more general cases with different viscosity ratios. According to the results, by increasing the ratio of the viscosity of the advancing phase to the viscosity of the receding phase, the dynamic contact angle reaches more quickly to its final value. It was also seen that by increasing the ratio of the length to the diameter of the tube the evolution of the dynamic contact angle becomes slower. The most interesting point is that a unique behavior is seen and a master curve is achieved if the time becomes dimensionless with a changing parameter (not a fixed parameter). This facilitates the way to predict and interpret the dynamic contact angle in the most general way.

Keywords: Capillary number, Microfluidics, Dynamic contact angle, Static contact angle, Surface tension

[1] Corresponding Author Email: mm.kamyabi@vru.ac.ir

Journal of Chemical and Petroleum Engineering
10.22059/jchpe.2021.318146.1346

1. INTRODUCTION

Different fluids exhibit different behaviors in contact with solid surfaces. These differences are due to the difference in their willingness to wet the solid surface. This tendency is called the fluid wetting or surface wettability. When two different immiscible (two phases) and static fluids are adjacent to the solid surface, the difference in their wettability results in a contact angle (θ) as shown in Fig. 1.

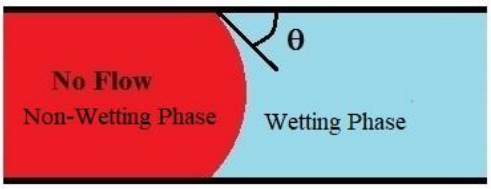

Fig. 1. The schematic of the contact line between two fluids and the observed contact angle

When the two fluids are stationary, the observed contact angle is called the static contact angle *(θ_s)*. The static contact angle is well known and computable based on the Young-Laplace equation. In the relative motion state of the phases and the solid surface, the contact angle is again observed and is called the dynamic contact angle (θ_d) which its quantity is different from the static one depending on different factors (1). In the relative motion mode of the phases, one phase moves forward and the other phase is naturally pushed back. Hence, for each CL between the two phases, there will be two advancing and receding contact angles.

Many researchers have investigated the dynamic contact angle, most of which experimental studies (2-5). These studies provide relations to predict the dynamic contact angle. However, as some of the most important ones will be shown below, they able to only predict the dynamic contact angle in a limited range. A number of studies concluded that the dynamic contact angle is dependent on some large-scale flow parameters such as the capillary number (6-8) and others believe that such a study should be conducted in the micro-scale by the use of molecular dynamics (9). The difference between apparent and microscopic dynamic contacts was highlighted by Omori and Kajishima (10)

Hoffman (7) designed a device to measure the dynamic contact angle observed in a liquid-air flow passing through a capillary tube. He did it for several different liquids and obtained the results for a relatively wide range of conditions, covering both viscous and inertial dominated regimes. The results of this work showed that the advancing contact angle in the liquid-air flow is a function of the Capillary number and the static contact angle and a universal function. The well-known law of Hoffman-Tanner suggests that for a completely wetting fluid (*i.e.*, the static contact angle is approximately zero) the dynamic contact angle follows the relation of $\theta_d^3 = 9Ca$ where *Ca* is the capillary number. This relationship holds for small contact angles (11). Also, when the static contact angle is not zero, the well-known Hoffman-Vinoff-Tanner relation was found applicable as $\theta_d^3 - \theta_s^3 = 72Ca$, although its constant is in principle slightly dependent on the size of the flow system (12).

Jiang et al. (13) collected various available data for the dynamic contact angle and provided the Eq. 1 for predicting the dynamic contact angle for the viscous flow regime:

$$\frac{\cos\theta_s - \cos\theta_d}{\cos\theta_s + 1} = \tanh(4.96\,Ca^{0.702}) \quad (1)$$

Bracke et al. (14) also obtained the Eq. 2 based on the results of a series of their own experiments:

$$cos\,\theta_d = cos\,\theta_s - 2(1 + cos\theta_s)Ca^{1/2} \quad (2)$$

As it is clear, although many experimental studies were conducted to investigate the dynamic contact angle, no definitive and exact relationship has been derived yet from laboratory data that is true for all materials in all geometrical and physical conditions. Moreover, it has been shown that such relations are not applicable to predict the dynamic contact angle, especially at relatively high Capillary numbers (12, 15). All this adds up to the fact that laboratory measurements of dynamic contact angles are very difficult, especially at points very close to the CL.

Modeling is another way to study the dynamic contact angle. The major difficulty encountered in modeling the shape of the CL (and therefore the contact angle) is the application of the no-slip wall boundary condition (which is a reasonable and widely used boundary condition for large-scale modeling) for such fluid-fluid-solid interface geometries which are very small in scale. This leads to the singularity in equations right at the CL and consequently, the solution diverges (11, 16). This issue was solved in different modeling works, by supposing that there is a slip in very close distances of the CL; e.g. distances less than *S* (17, 18). However, no convincing experiment or theory has yet been found to support or reject these kinds of methods (9).

Cox(17) developed an approximate method and assumed that in the distances less than *S* (slip length) the dynamic contact angle tends to the static contact angle, and finally reached to Eq. 3:

$$g(\theta_d, M) - g(\theta_s, M) = Ca\,[\ln(\varepsilon^{-1}) + Q] + O(Ca^2) \quad (3)$$

where $\varepsilon = S/R$, Q depends on the slip model and imposed boundary condition, g is a simple function which tends to the Hoffman universal function as viscosity ratio of the fluids tends to the infinity.

Eggers and Stone (11) showed the importance of the characteristic lengths in the prediction of the dynamic contact angle. They concluded that for the full wetted state (i.e., when θ_s=0), the dynamic contact angle at a distance of *x* from the CL is predicted with the Eq. 4:

$$\theta_d^3(x) = 9Ca\,ln(\frac{x}{S}ca^{\beta}) \quad (4)$$

where β is a positive constant and is dependent on the type of the physical slip mechanism (such as Van der Waals, Navier slip, nonlinear slip, etc.) which is assumed to be applicable at the locations very close to the CL (distances less than *S*). Although this relation provides a good physical view of the dynamic contact angle, it has a great deal of uncertainty due to the how the β constant and the microscope length (*S*) are taken into account.

Accurate prediction of most of large-scale models is dependent on some micro-scale parameters such as slip length (*S*). Hence, microscale (molecular) models were mostly dedicated to predicting the slip length. These models were also used to predicting the relationship of dynamic contact angle with flow velocity or Capillary number (19, 20). They have also been developed in order to predict the effects of the uneven solid surfaces on the dynamic contact angle (21).

As it was seen, most studies on the dynamic contact angle considered the steady flow of a case of two-phase liquid-air. It means the viscosity of one phase was deliberately ignored in comparison with the other phase. However, by conducting experiments on the two-phase flows of different liquid-air and liquid-liquid systems, Fermigier and Jenffer (22) found that their results of dynamic contact angle for liquid-air systems are in good agreement with the well-known Hoffman-Tanner relation as well as Cox's theory predictions, but the data obtained for the dynamic contact angle in liquid-liquid systems was greater than predictions by existing theories. Actually, they noticed the influence of the viscosity ratio of the phases (*i.e.*, the effect of the Capillary number of both phases) on the dynamic contact angle.

According to what is known so far, the effects of viscosity ratio and characteristic lengths on the dynamic contact angle should not be underestimated by the capillary number of only one phase. However, no definitive theoretical equation or comprehensive experimental relationship has yet been derived that encompasses all these parameters together. The current study tried to start the development of such a relation although with some simplification assumptions at the first. The model considers the two phases separately and starts with the popular Hagen-Poiseuille equation for the single-phase flows in tubes and the equivalent equation for the channels. This idea was first suggested by Washburn (23) and then widely used in a series of publications by Hilpert (24-27) where the liquid infiltration into and liquid withdrawal from capillary tubes were modeled. Using the Young-Laplace equation for predicting the contact angle as the function of pressure drop across the CL, the model was completed to obtain the final relation for the dynamic contact angle. Cai et al. (28, 29) also used the same idea for predicting the spontaneous imbibition in capillaries. Although these studies examined different geometric and physical states in great detail, the viscosity of the second phase was ignored. They also assumed the pressure difference between the two ends of the capillary to be zero and used the experimental models mentioned earlier to predict the dynamic contact angle. However, in the present study, this problem is tried to be investigated in its most general case of two-phase flow without mentioned limitations. The effects of the viscosity ratio and characteristic length ratio will be quantified for the first time.

2. THEORY

According to Fig. 2, it was assumed that the two fluids flow from left to right in a capillary channel and a capillary tube. The dynamic contact angle was defined as the contact angle between the wetting fluid (e.g. fluid 1) and the solid surface as shown in this figure. P_1, P_2, P_3, and P_4 were the pressures at the places shown on this figure.

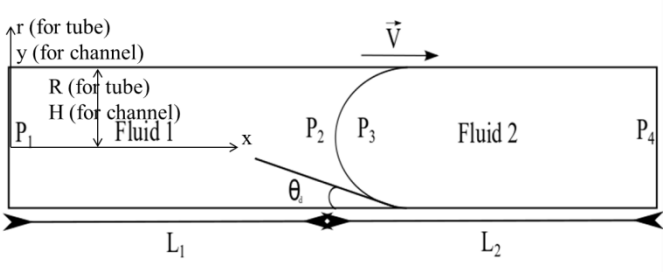

Fig. 2. The simplified geometries of the channel flow and the tube flow

To study the fluids flow in such conditions, the following assumptions were intended:

1. Fluids are immiscible and fluid 1 (according to Fig. 1) is the wetting phase.

2. Fluids are Newtonian and flows are incompressible (Because of low Mach number).

3. The surface tension between the fluids as well as between the fluid and the solid wall is constant.

4. The flows are laminar (*i.e.*, the viscous regime is dominant due to low Reynolds numbers).

5. The pressure at each point of any cross-sectional area is constant and only changes along the channel/tube length.

6. The flows are fully developed and the pressure changes linearly in each phase.

7. Gravity is neglected (Because the Bond number ($Bo = \frac{(P_1-P_4)gL^2}{\sigma}$) is low for such assumed microscale flows).

8. The interface moves at a constant velocity

9. Fluids flow from left to right at a quasi-steady-state condition.

Applying Navier-Stokes equations in the flow direction for each fluid, by considering the above assumptions, along with using mass conservation equation, the Eq. 5 and the Eq. 6 are obtained:

$$\text{For channel flow: } \begin{cases} \text{for fluid 1: } \frac{P_1-P_2}{L_1} + \mu_1 \frac{d^2u_1}{dy^2} = 0 \\ \text{for fluid 2: } \frac{P_3-P_4}{L_2} + \mu_2 \frac{d^2u_2}{dy^2} = 0 \end{cases} \quad (5)$$

$$\text{For tube flow: } \begin{cases} \text{for fluid 1: } \frac{P_1-P_2}{L_1} + \frac{\mu_1}{r}\frac{d}{dr}\left(r\frac{du_1}{dr}\right) = 0 \\ \text{for fluid 2: } \frac{P_1-P_2}{L_2} + \frac{\mu_2}{r}\frac{d}{dr}\left(r\frac{du_2}{dr}\right) = 0 \end{cases} \quad (6)$$

Supposing that no-slip boundary condition is valid on the wall surfaces for both fluids, the solutions of equations 5 and 6 are the Eq. 7 and Eq. 8:

$$\text{For channel flow: } \begin{cases} P_1 - P_2 = \frac{3\bar{U}L_1\mu_1}{H^2} \\ P_3 - P_4 = \frac{3\bar{U}L_2\mu_2}{H^2} \end{cases} \quad (7)$$

$$\text{For tube flow: } \begin{cases} P_1 - P_2 = \frac{8\mu_1 L_1 \bar{U}}{R^2} \\ P_3 - P_4 = \frac{8\mu_2 L_2 \bar{U}}{R^2} \end{cases} \quad (8)$$

where $\bar{U}$ is the average velocity of the fluids inside the tube/channel. Since the average velocity is the same for the both fluids, it has no indexes. As it was expected, the obtained equation for the capillary tube flow is the popular equation of Hagen-Poiseuille.

Now, by applying force balance to the CL and using the Young-Laplace equation, the Eq. 9 and the Eq. 10 are obtained:

For channel flow: $P_2 - P_3 = -\frac{\sigma\cos(\theta_d)}{H}$ (9)

For tube flow: $P_2 - P_3 = -\frac{2\sigma\cos(\theta_d)}{R}$ (10)

By adding equations 9 and 10 to equations 7 and 8 respectively, the following equations 11 and 12 are derived:

For channel flow: $cos(\theta_d) = \frac{3}{H}(Ca_2 L_2 + Ca_1 L_1) - \frac{(P_1 - P_4)H}{\sigma}$ (11)

For tube flow: $cos(\theta_d) = \frac{4}{R}(Ca_2 L_2 + Ca_1 L_1) - \frac{(P_1 - P_4)R}{2\sigma}$ (12)

where $Ca_1 = \frac{\mu_1 \bar{U}}{\sigma}$ and $Ca_2 = \frac{\mu_2 \bar{U}}{\sigma}$ mean the Capillary numbers based on the viscosities of fluids 1 and 2 respectively.

The terms $\frac{(P_1 - P_4)H}{\sigma}$ and $\frac{(P_1 - P_4)R}{2\sigma}$ can be assumed as the dimensionless pressure differences in the whole of the channel and the tube respectively. Therefore, equations 11 and 12 show an explicit relationship among the dynamic contact angle observed in the channel/tube, the dimensionless pressure differences between the two sides of the channel/tube, the Capillary numbers of both phases and the characteristic lengths of the channel/tube. Equations 11 and 12 are the main ones and all the following relations developed for the dynamic contact angle are based on these two equations.

As a simpler case, the length of the channel/tube (L_1+L_2) can be assumed long. Therefore, it can be assumed that L_1=L_2≅L and they are not changed notably at small time intervals. Therefore equations 11 and 12 convert to the equations 13 and 14 as:

For channel flow: $cos(\theta_d) = \frac{3L}{H}(Ca_2 + Ca_1) - \frac{(P_1 - P_4)H}{\sigma}$ (13)

For tube flow: $cos(\theta_d) = \frac{4L}{R}(Ca_2 + Ca_1) - \frac{(P_1 - P_4)R}{2\sigma}$ (14)

Equations 13 and 14 are valid at the conditions were steady assumption is not far from reality. However, these equations demonstrate vividly the effect of the ratio of the characteristic lengths (L/H for the channel and L/R for the tube) on the dynamic contact angle.

However, in transient conditions, as the fluids flow through the channel/tube, the lengths of L_1 and L_2 changes so that at a certain time of t from the beginning of the flow, $L_1 = L_{1,0} + \bar{U}t$ and $L_2 = L_{2,0} - \bar{U}t$ where $L_{1,0}$ and $L_{2,0}$ are the initial values of L_1 and L_2 respectively. Therefore, equations 11 and 12 convert to the equations 15 and 16 respectively:

For channel flow: $cos(\theta_d) = \frac{3}{H}[Ca_2(L_{2,0} - \bar{U}t) + Ca_1(L_{1,0} + \bar{U}t)] - \frac{(P_1 - P_4)H}{\sigma}$ (15)

For tube flow: $\cos(\theta_d) = \frac{4}{R}[Ca_2(L_{2,0} - \bar{U}t) + Ca_1(L_{1,0} + \bar{U}t)] - \frac{(P_1 - P_4)R}{2\sigma}$ (16)

Using weather Eqs. 13,14 or Eqs. 15,16 depends on the real test conditions (steady or transient) which one may apply in the laboratory to obtain data. However, we continue with the Eqs. 13 and 14 hereafters although all following equations can also be re-derived for Eqs. 15 and 16.

It is expected that the fluids do not flow for a certain value of pressure difference between the two ends of the channel/tube (e.g., for P_4-P_1 = P_3-P_2= $\Delta P_{st\text{-}lr}$). For the pressure differences (P_4-P_1) less than $\Delta P_{st\text{-}lr}$ the fluids flow from left to the right and for the pressure differences higher than $\Delta P_{st\text{-}lr}$ the fluids flow from right to the left. According to this argument, at the states that the fluids do not flow (where P_4-P_1 = $\Delta P_{st\text{-}lr}$), the pressure difference can be related to the static contact angle using the Young-Laplace relation as equations 17 and 18:

For channel flow: $\Delta P_{st-lr} = \frac{\sigma cos(\theta_s)}{H}$ (17)

For tube flow: $\Delta P_{st-lr} = \frac{2\sigma cos(\theta_s)}{R}$ (18)

Normally, for the general situations where the fluids are either flowing from left to right or they are stationary, the pressure difference can be written as Eq. 19:

P_1-P_4 = - $\Delta P_{st\text{-}lr}$ + ΔP_D (19)

where $\Delta P_D \geq 0$. (ΔP_D=0 means the fluids do not flow)

Therefore, by substituting equations 17, 19 in Eq. 13 and equations 18, 19 in Eq. 14, the equations 20 and 21 are derived:

For channel flow: $cos(\theta_d) - cos(\theta_s) = \frac{3L}{H}(Ca_2 + Ca_1) - \frac{H\Delta P_D}{\sigma}$ (20)

For tube flow: $cos(\theta_d) - cos(\theta_s) = \frac{4L}{R}(Ca_2 + Ca_1) - \frac{R\Delta P_D}{2\sigma}$ (21)

For the cases where $Ca_2 \ll Ca_1$ (e.g., the viscosity of the receding fluid (μ_2) is negligible in comparison with the viscosity of the advancing fluid (μ_1)), the equations simplify to equations 22 and 23:

For channel flow: $cos(\theta_d) - cos(\theta_s) = \frac{3LCa_1}{H} - \frac{H\Delta P_D}{\sigma}$ (22)

For tube flow: $cos(\theta_d) - cos(\theta_s) = \frac{4LCa_1}{R} - \frac{R\Delta P_D}{2\sigma}$ (23)

And for the cases where $Ca_1 \ll Ca_2$ (e.g. the viscosity of the advancing fluid (μ_1) is negligible in comparison with the viscosity of the receding fluid (μ_2)), the equations are simplified to equations 24 and 25:

For channel flow: $cos(\theta_d) - cos(\theta_s) = \frac{3LCa_2}{H} - \frac{H\Delta P_D}{\sigma}$ (24)

For tube flow: $cos(\theta_d) - cos(\theta_s) = \frac{4LCa_2}{R} - \frac{R\Delta P_D}{2\sigma}$ (25)

All the above equations for θ_d, make a relation among three unknown parameters of dynamic contact angle, pressure difference, and average velocity. Therefore, another two relations are

needed among these three variables in order to close the system of equations. One additional equation can be the same as the experimental relationships obtained for the dynamic contact angle, some of which were mentioned in the introduction section (*e.g.*, equations 1, 2). Moreover, almost all previous researches have considered the conditions in such a way that the pressure at the inlet and outlet of the capillary is the same as the atmospheric pressure and as a result one of the unknowns have been also removed (because $P_1 - P_4 = 0$). Therefore, the system of equations can be solved now with two remained unknowns and two equations.

3. MODEL VALIDATION

Hilpert (24) solved the quasi-steady problem of liquid infiltration into a capillary tube where it was assumed that the initial dynamic contact angle was 90^0 ($\theta_{d,0} = 90^0$), $L_{1,0}=0$, $P_1 - P_4 = 0$ and $\theta_s = 40^0$. Because of the low viscosity of the air (as the receding phase), a single-phase flow was assumed by Hilpert (24). The same problem was solved numerically by combining Bracke's model (Eq. 2) with Eq. 16 by assuming that $Ca_2 \ll Ca_1$. This was because the viscosity of the air is much lower than the liquid.

Fig. 3 compares the results of the obtained dynamic contact angle as a function of dimensionless time ($\tau = \frac{t\sigma}{\mu R}$) between the present work and Hilpert's study (24). As it is clear, the results are in fair agreement. This approves the validity of the present method. The results obtained by Li et al. (30) were also shown in the same figure.

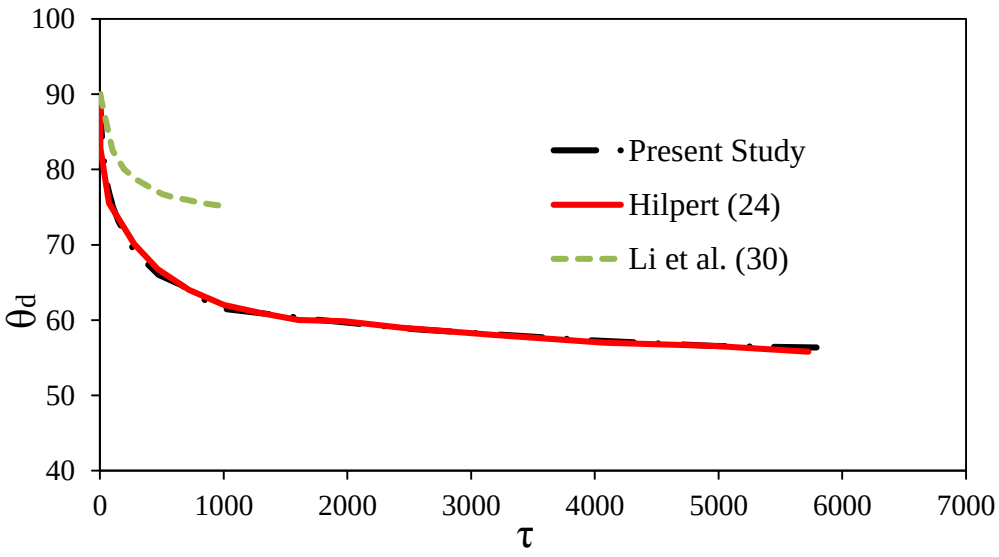

Fig. 3. Comparison among the results of the present study for the dynamic contact angle as a function of dimensionless time with the results of Hilpert (24) and Li et al. (30)

By proving the validity of the model, it was used for a variety of situations.

4. RESULTS AND DISCUSSION

Equations 11 and 12 show relations in the most general way for the dynamic contact angles observed in a two-phase flow inside the capillary channel and tube respectively. According to these equations, the dynamic contact angle is a function of the dimensionless pressure differences between the two ends of the channel/tube, the Capillary numbers of both phases, and the characteristic lengths of the channel/tube. It is necessary to mention that the pressure

difference (P_1-P_4), the average velocity ($\bar{U}$) and the contact angle (θ_d) are not independent of each other. Actually, according to these relations, an increase in P_1-P_4 is compensated by the tolerable decrease in the dynamic contact angle (θ_d) and an increase in the value of the average velocity of the flows ($\bar{U}$). However, the main point is that the instantaneous values of these variables definitely satisfy equations 11 and 12 for the channel and the tube, respectively.

Equations 13 and 14 express the same relations for the steady flows and equations 15 and 16 do the same for the time-dependent flows. Equations 20 and 21 provide a clearer picture of the relationship between the dynamic (θ_d) and the static (θ_s) contact angles. Equations 22 to 25 simplify the mentioned relations for the special cases where the Capillary number of one of the fluids is much lower than the other one.

Showing the results obtained by these equations in graphical format is useful. Therefore, in following the effects of viscosity ratio and length to radius ratio on the dynamic contact angle will be discussed.

4.1 Effect of Viscosity Ratio

Unlike the single-phase flows, no experimental relation has been provided so far to predict the dynamic contact angle in two-phase flows with comparable viscosities. Therefore, solving equations 11 and 12 is not possible in its general form because of the smaller number of equations (equal to 1) than the variables (equal to 3). However, it is possible to reduce the variables by investigating a simpler case where $P_1 - P_4 = 0$. For such a case still two unknowns (θ_d and $\bar{U}$) exist. As a simple first-order estimation, it is possible to assume that Bracke's model (Eq.2) is still usable. However, Bracke's model is dedicated to the tube flows. Therefore, only Eq. 12 was solved numerically for such a case and the results are shown in Figs. 4 to 8.

In Figs. 4 to 6, the evolution of the dynamic contact angle inside a tube is shown versus dimensionless time at different values of viscosity ratios of the phases (μ_1/μ_2) for initial values of $\theta_{d,0} = 90^0, 75^0, 60^0$ respectively. The static contact angle (θ_s) was equal to 40^0 for all these cases. As it is clear, with increasing in viscosity ratio (μ_1/μ_2), the evolution of the contact angle with dimensionless time become faster. In fact, when the first fluid does not change (means constant values of μ_1) while the second fluid becomes less viscous, the dynamic contact angle changes occur faster to reach the final value. This is because the resistance against the flow in the second phase decreases by decrease of μ_2.

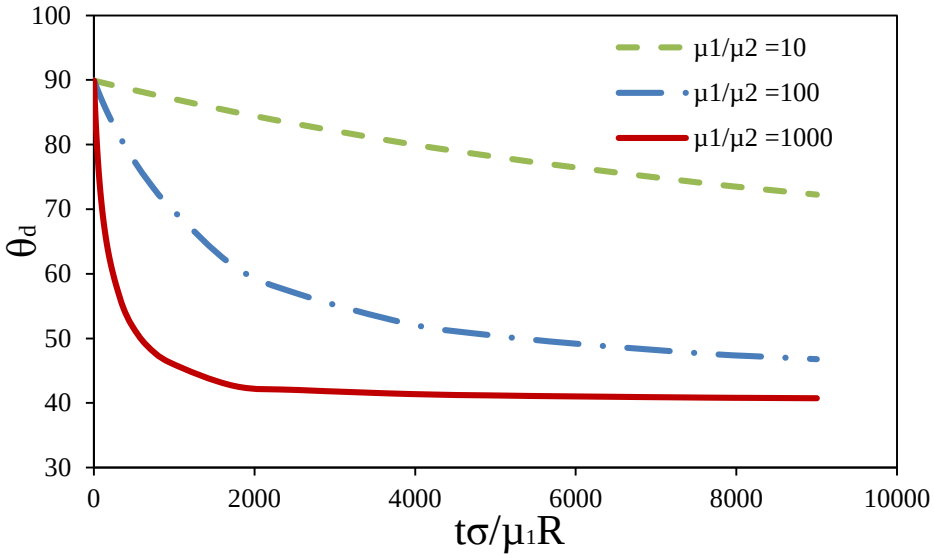

Fig. 4. Dynamic contact angle in a tube as a function of dimensionless time for different values of μ_1/μ_2 for a case with initial dynamic contact angle of 90^0

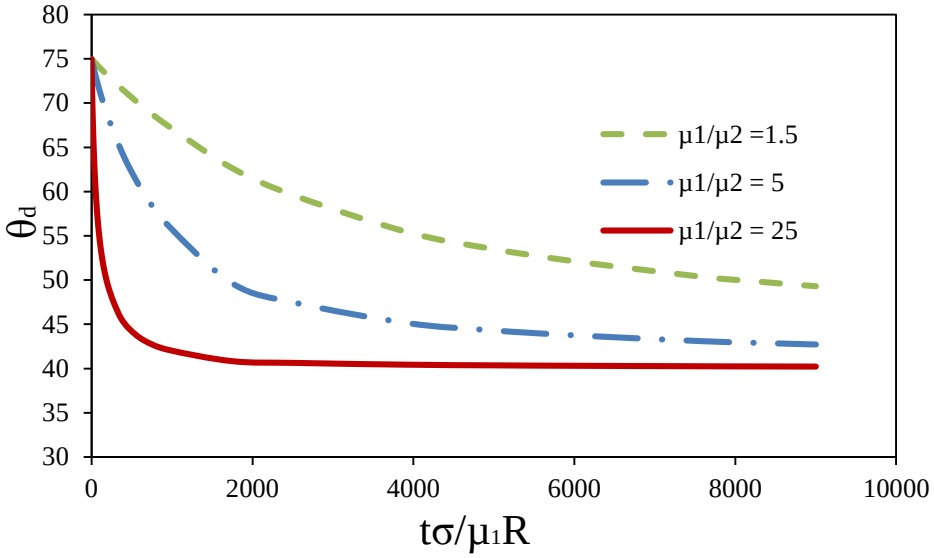

Fig. 5. Dynamic contact angle in a tube as a function of dimensionless time for different values of μ_1/μ_2 for a case with initial dynamic contact angle of 75^0

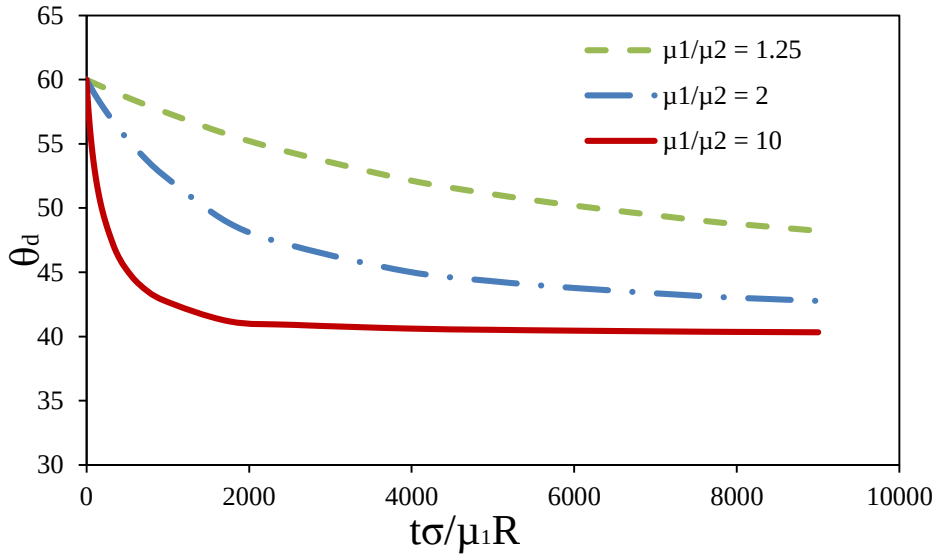

Fig. 6. Dynamic contact angle in a tube as a function of dimensionless time for different values of μ_1/μ_2 for a case with initial dynamic contact angle of 60^0

For all those cases shown in Figs. 4 to 6, the time was become dimensionless by the value of μ_1 as a constant parameter. However, the time can become dimensionless by using μ_2 (as a changing parameter) instead of μ_1. Fig. 7 shows such data for a case of initial dynamic contact angle of 90^0 and static contact angle of 40^0. Comparing Fig.7 with Fig. 4, the graphs with different values of μ_1/μ_2 are superimposed and the differences are faded. This in fact indicates that although by keeping μ_1 constant and μ_2 decreasing, the real time of equilibrium decreases, these differences if examined in the context of dimensionless time by the changing factor (here μ_2) will disappear. Actually, a master curve is obtained that summarizes all the data. Other master curves can also be achieved for the data shown in Figs. 5 and 6.

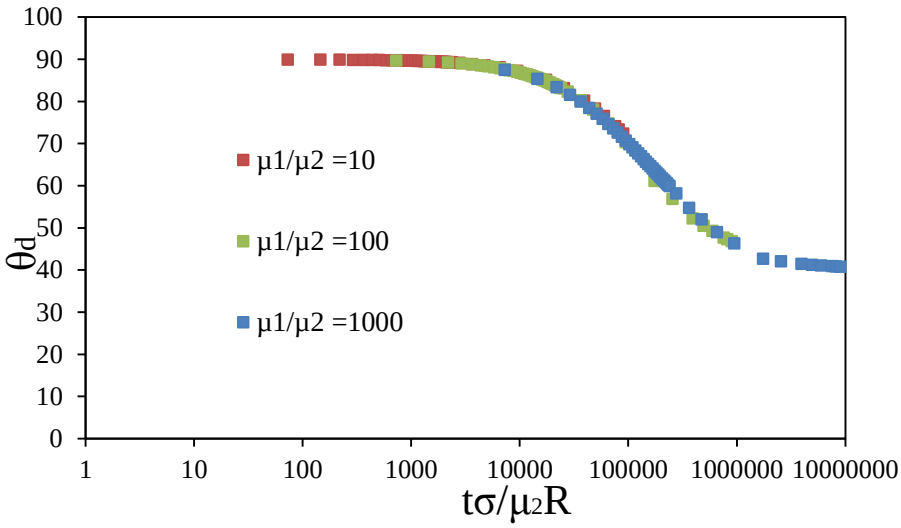

Fig. 7. Dynamic contact angle in a tube when the time has become dimensionless with the changing parameter (here μ_2)

4.2. Effect of Length Ratio

Characteristic lengths are also effective parameters on the dynamic contact angle according to Eqs. 11 and 12. Fig. 8 shows the effect of the ratio of length to the diameter of the tube ($^{L}/_{R}$) on the evolution of the dynamic contact angle for a case with $\theta_{d,0} = 90^0$ and $^{\mu_1}/_{\mu_2} = 100$. According to this figure, increasing the value of $^{L}/_{R}$ leads to a slower process of reduction of the contact angle with time. Actually, for the tubes with larger $^{L}/_{R}$ ratios, the contact angle has more time to change from its initial value to its final value.

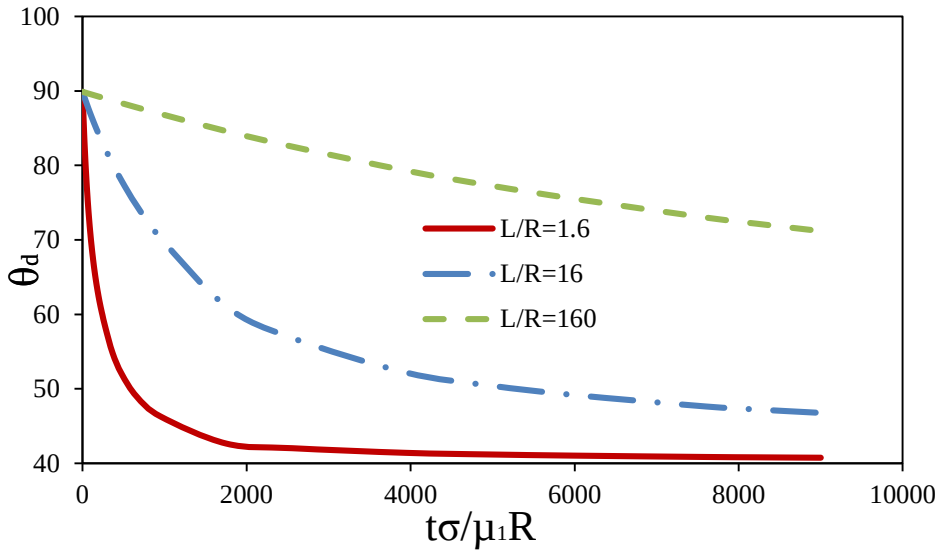

Fig. 8. Dynamic contact angle in a tube as a function of dimensionless time for different values of $^{L}/_{R}$ for a case with initial dynamic contact angle of 90^0

The same data are shown in Fig.9 but the time was become dimensionless by the length of the tube (L) rather than its radius (R). Again a master curve is observed. It is needed to notice that L was the changing parameter in all the graphs.

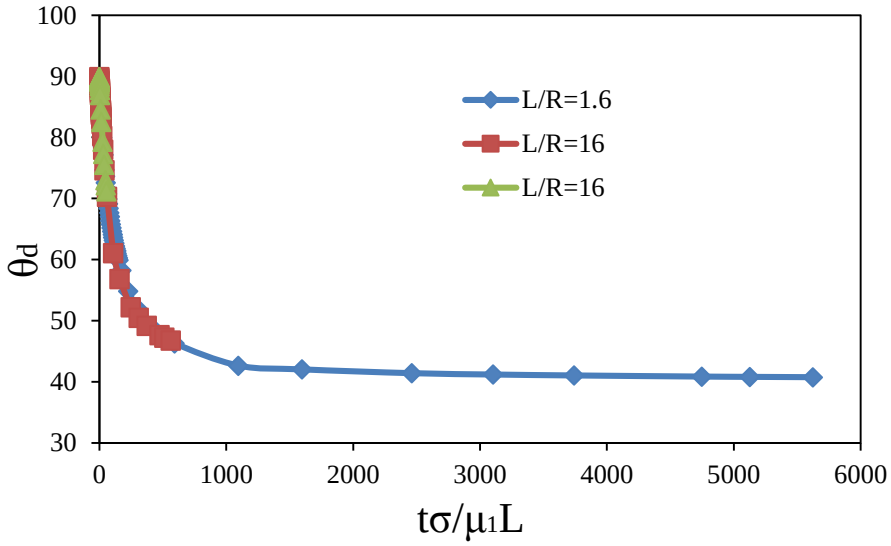

Fig. 9. Dynamic contact angle in a tube when the time has become dimensionless with the changing parameter (here L)

According to Figs. 7 and 9, it can be claimed that a master curve and a unique behavior is expected for the evolution of the dynamic contact with the dimensionless time if the time was become dimensionless by the changing parameter.

5. CONCLUSION

In the present study, using a simplified mathematical model based on the Navier-Stokes equations, along with the use of the Young-Laplace equation, the problem of quasi steady motion of the contact line between two immiscible fluids within a capillary channel and a capillary tube was solved. For this model, several common assumptions including Newtonian fluid, incompressible, laminar, and fully developed flow were assumed. In addition, the quasi steady-state condition and linear pressure drop for each fluid along the channel/tube were assumed. The effect of gravity was also ignored due to the low Bond number.

Based on the model predictions, it was found that the dynamic contact angle observed in a two-phase flow has a direct relation with the dimensionless pressure difference between the two ends of the channel/tube, the Capillary numbers of both phases as well as the ratio of the geometric characteristic lengths of the channel ($^{L}/_{H}$) and of the tube ($^{L}/_{R}$). The effects of these parameters, although some of them were previously qualitatively proven, were never explicitly expressed quantitatively before. It was also useful to divide the term of the dimensionless pressure difference to the two terms of the static contact angle and the remaining pressure. This clarifies the role of the static contact angle in determining the dynamic contact angle.

The model was validated through a comparison of its results for the dynamic contact angle versus dimensionless time for a case of water-air flow with the literature data. After validation, it was applied for situations with different viscosity ratios ($^{\mu_1}/_{\mu_2}$) and different characteristic length ratios ($^{L}/_{R}$). It was found that the evolution of the dynamic contact angle (from the initial value to the equilibrium value) slows down with decreasing in μ_1/μ_2 and vice versa. However, it was found that if the time becomes dimensionless with the changing parameter (here μ_2), a master curve is obtained that holds all the data together. Also, it was seen that with increasing the value of the ratio of the length to the radius of the tube ($^{L}/_{R}$), the evolution of the dynamic contact angle slows down. Again a master curve was obtained when the time was become dimensionless by the changing parameter (here L). Finding master curves facilitates the way to predict and interpret the dynamic contact angle results that may be obtained in a variety of experimental or modeling ways.

The presented model proves that in a two-phase flow inside a confined media (*e.g.* a tube or channel), the changes in the time context of the dynamic contact angle are not only influenced by the properties (*e.g.* viscosity or *Ca* number) of the advancing phase but also by the properties of the receding phase. Moreover, the characteristic length ratios are also effective parameters on the evolution of the dynamic contact angle. These findings although came from a simplified model and a first-order solution, make new insights into the understanding of the evolution of the dynamic contact angle in two-phase microscale flows.

NOMENCLATURE

Nomenclature should be in alphabetic order (A – Z) and Greek letters should follow after Latin letters in alphabetic *order (α β ...)*

Bo	Bond number	t	time
Ca	Capillary number	$\bar{U}$	average velocity of the fluid
Ca_1	Capillary number of fluid 1	u_1	velocity of fluid 1
Ca_2	Capillary number of fluid 2	u_2	velocity of fluid 2
H	half the width of the channel	g	gravity acceleration
L_1	channel/tube length of the left side	β	a constant in Eq. 4
$L_{1,0}$	initial value of L_1	$\Delta P_{st\text{-}lr}$	pressure difference at which fluids do not flow
L_2	channel/tube length of the right side	ΔP_D	remaining pressure difference
$L_{2,0}$	initial value of L_2	θ_d	dynamic contact angle
P_1	pressure at the inlet	$\theta_{d,0}$	initial value of dynamic contact angle
P_2	pressure at the left side of the interface	θ_s	static contact angle
P_3	pressure at the right side of the interface	μ_1	viscosity of fluid 1
P_4	pressure at the outlet	μ_2	viscosity of fluid 2
R	radius of the tube	σ	surface tension coefficient
r	radial coordinate		
S	microscopic length		
y	y-component of Cartesian coordinate		

REFERENCES

1. Prokopev S, Vorobev A, Lyubimova T. Phase-field modeling of an immiscible liquid-liquid displacement in a capillary. Physical Review E. 2019;99(3):033113.
2. Wu P, Nikolov AD, Wasan DT. Capillary rise: validity of the dynamic contact angle models. Langmuir. 2017;33(32):7862-72.
3. Liu J, Sheng JJ, Wang X, Ge H, Yao E. Experimental study of wettability alteration and spontaneous imbibition in Chinese shale oil reservoirs using anionic and nonionic surfactants. Journal of Petroleum Science and Engineering. 2019;175:624-33.
4. Blake T, Batts G. The temperature-dependence of the dynamic contact angle. Journal of colloid and interface science. 2019;553:108-16.
5. Wang X, Min Q, Zhang Z, Duan Y, Zhang Y, Zhai J. Influence of head resistance force and viscous friction on dynamic contact angle measurement in Wilhelmy plate method. Colloids and Surfaces A: Physicochemical and Engineering Aspects. 2017;527:115-22.
6. Burley R, Jolly RP. Entrainment of air into liquids by a high speed continuous solid surface. Chemical Engineering Science. 1984;39(9):1357-72.
7. Hoffman RL. A study of the advancing interface. I. Interface shape in liquid—gas systems. Journal of colloid and interface science. 1975;50(2):228-41.
8. Wilson S. A note on the measurement of dynamic contact angles. Journal of Colloid and Interface Science. 1975;51(3):532-4.
9. Thompson PA, Robbins MO. Simulations of contact-line motion: slip and the dynamic contact angle. Physical Review Letters. 1989;63(7):766.
10. Omori T, Kajishima T. Apparent and microscopic dynamic contact angles in confined flows. Physics of Fluids. 2017;29(11):112107.
11. Eggers J, Stone HA. Characteristic lengths at moving contact lines for a perfectly wetting fluid: the influence of speed on the dynamic contact angle. Journal of Fluid Mechanics. 2004;505:309-21.
12. Šikalo Š, Wilhelm H-D, Roisman I, Jakirlić S, Tropea C. Dynamic contact angle of spreading droplets: Experiments and simulations. Physics of Fluids. 2005;17(6):062103.
13. Jiang T-S, Soo-Gun O, Slattery JC. Correlation for dynamic contact angle. Journal of colloid and interface science. 1979;69(1):74-7.

14. Bracke M, De Voeght F, Joos P. The kinetics of wetting: the dynamic contact angle. Trends in Colloid and Interface Science III: Springer; 1989. p. 142-9.
15. Kamyabi A, SA AR, Kamyabi M. Surfactant effects on the efficiency of oil sweeping from the dead ends: Numerical simulation and experimental investigation. Chemical Engineering Research and Design. 2015;94:173-81.
16. De Gennes P-G. Wetting: statics and dynamics. Reviews of modern physics. 1985;57(3):827.
17. Cox R. The dynamics of the spreading of liquids on a solid surface. Part 1. Viscous flow. Journal of fluid mechanics. 1986;168:169-94.
18. Hocking L. A moving fluid interface. Part 2. The removal of the force singularity by a slip flow. Journal of Fluid Mechanics. 1977;79(2):209-29.
19. Blake TD. The physics of moving wetting lines. Journal of colloid and interface science. 2006;299(1):1-13.
20. De Ruijter MJ, Blake T, De Coninck J. Dynamic wetting studied by molecular modeling simulations of droplet spreading. Langmuir. 1999;15(22):7836-47.
21. Rolley E, Guthmann C. Dynamics and hysteresis of the contact line between liquid hydrogen and cesium substrates. Physical review letters. 2007;98(16):166105.
22. Fermigier M, Jenffer P. An experimental investigation of the dynamic contact angle in liquid-liquid systems. Journal of colloid and interface science. 1991;146(1):226-41.
23. Washburn EW. The dynamics of capillary flow. Physical review. 1921;17(3):273.
24. Hilpert M. Effects of dynamic contact angle on liquid infiltration into horizontal capillary tubes:(Semi)-analytical solutions. Journal of colloid and interface science. 2009;337(1):131-7.
25. Hilpert M. Effects of dynamic contact angle on liquid withdrawal from capillary tubes:(Semi)-analytical solutions. Journal of colloid and interface science. 2010;347(2):315-23.
26. Hilpert M. Explicit analytical solutions for liquid infiltration into capillary tubes: Dynamic and constant contact angle. Journal of colloid and interface science. 2010;344(1):198-208.
27. Hilpert M. Liquid withdrawal from capillary tubes: explicit and implicit analytical solution for constant and dynamic contact angle. Journal of colloid and interface science. 2010;351(1):267-76.
28. Cai J, Perfect E, Cheng C-L, Hu X. Generalized modeling of spontaneous imbibition based on Hagen–Poiseuille flow in tortuous capillaries with variably shaped apertures. Langmuir. 2014;30(18):5142-51.
29. Cai J, Hu X, Standnes DC, You L. An analytical model for spontaneous imbibition in fractal porous media including gravity. Colloids and Surfaces A: Physicochemical and Engineering Aspects. 2012;414:228-33.
30. Li C, Shen Y, Ge H, Zhang Y, Liu T. Spontaneous imbibition in fractal tortuous micro-nano pores considering dynamic contact angle and slip effect: phase portrait analysis and analytical solutions. Scientific reports. 2018;8(1):1-13.